
Fast vehicle detection algorithm based on lightweight YOLO7-tiny

Bo Li^a, YiHua Chen^a and Hao Xu ^{a,*}

^a School of Mechanical Engineering, Hubei University of Technology, Wuhan 430000, China;

* Correspondence to: Hao Xu (chrisgank12138@gmail.com)

Abstract: The swift and precise detection of vehicles holds significant research significance in intelligent transportation systems (ITS). However, current vehicle detection algorithms encounter challenges such as high computational complexity, low detection rate, and limited feasibility on mobile devices. To address these issues, this paper proposes a lightweight vehicle detection algorithm for YOLOv7-tiny called Ghost-YOLOv7. The model first scales the width multiple to 0.5 and replaces the standard convolution of the backbone network with Ghost convolution to achieve a lighter network and improve the detection speed; secondly, a Ghost bi-directional feature pyramid network (Ghost-BiFPN) neck network is designed to enhance feature extraction capability of the algorithm and enrich semantic information; thirdly, a Ghost Decoupled Head (GDH) is employed for accurate prediction of vehicle location and class, enhancing model accuracy; finally, a coordinate attention mechanism is introduced in the output layer to suppress environmental interference, and the WIoU loss function is employed to enhance the detection accuracy further. Experimental results on the PASCAL VOC dataset demonstrate that Ghost-YOLOv7 outperforms the original YOLOv7-tiny model, achieving a 29.8% reduction in computation, 37.3% reduction in the number of parameters, 35.1% reduction in model weights, and 1.1% higher mean average precision (mAP), while achieving a detection speed of 428 FPS. These results validate the effectiveness of the proposed method.

Keywords: vehicle detection; lightweight; Ghost-YOLOv7; deep learning

1、Introduction

Nowadays, the pursuit of safety and comfort drives the development of autonomous driving technology. Self-driving cars are a revolutionary tool for road traffic and a significant indicator of human progress in this new era. Vehicle detection is one of the most critical technologies in autonomous driving research. [1] Vehicle detection methods can be broadly classified into traditional and deep learning-based approaches.

Earlier researchers utilized various features like edge information, color, and symmetry of vehicles to detect them in images. Tsai et al. [2] proposed a vehicle detection technique that used color and edges to detect vehicles from static images. Similarly, Chen et al. [3] developed a vision-based system for daytime brake light detection that extracts the symmetry verification of the headlight at night and combines brightness and radial symmetry to detect the brake light, which helped identify vehicles. As technology

progressed, more robust feature descriptors such as Scale Invariant Feature Transform (SIFT), Histogram of Oriented Gradients (HOG), and others [4-6] emerged, which were more effective than the previous edge features and local symmetry features. After manually designing features based on human perception of vehicles, Support Vector Machine (SVM) and AdaBoost classifiers were used for detection tasks. Cheng et al. [7] proposed a cascaded classifier that combined AdaBoost and SVM, extracting candidate regions from left to right and top to bottom of the image using a fixed-size window, followed by feature extraction and classification of candidate regions using a cascade classifier. Satzoda et al. [8] constructed Vehicle Detection using Active learning and Symmetry, a multipart-based vehicle detection algorithm that utilized active learning and symmetry, employing Haar features and Adaboost classifiers to detect fully and partially visible rear views of vehicles.

In contrast, Razalli et al. [9] presented a novel approach that combines HSV color segmentation and SVM to detect moving emergency vehicles in traffic cameras. Most of the above techniques use manual feature selection to design and train classifiers based on specific detection objects. However, these manual feature extraction methods usually extract overly homogeneous features and cannot accurately detect objects in complex traffic environments.

With the continuous advancement of deep learning technology, vehicle detection methods based on deep learning have emerged as a popular area of research. This deep learning-based vehicle detection approach can be divided into two categories using Convolutional Neural Networks (CNN) [10] and Vision Transformer (ViT). [11-12] Vision Transformer has become a significant hit in recent years due to its higher detection accuracy, but these models often sacrifice detection speed and are expensive. Sun et al. [13] introduced an effective vehicle detection method based on the swin transformer algorithm for vehicle detection in fuzzy scenes. The article proposes a new algorithm called a hazy detection transformer, which improves the swin transformer to enhance the performance of fuzzy backgrounds. Experimental results show that the algorithm provides good detection results in different datasets and scenarios and has better robustness and accuracy than other common vehicle detection algorithms. Deshmukh et al. [14] propose a swin transformer-based vehicle detection method for the lack of vehicle detection accuracy in a disordered traffic environment. The technique uses BiFPN to enhance the feature fusion capability. It uses a fully connected vehicle detection head to improve the matching relationship between vehicle size and BiFPN, effectively improving vehicle detection accuracy and robustness on various data sets.

CNN-based approaches for vehicle detection are typically faster, cheaper, and simpler to deploy models than ViT-based ones. Arora et al. [15] used the Faster R-CNN technique to detect vehicles in different daytime, nighttime, sunny and rainy conditions and achieved satisfactory results. Satyanarayana et al. [16] used spatiotemporal information obtained from CNN graphs for unsupervised vehicle detection, and the training dataset did not require any labels; the CNN was trained using road signs and acted as a background, the occupancy data was used as spatiotemporal information to approximate and classify the width and length of the vehicles, and the method achieved satisfactory accuracy. Zakaria et al. [17] used a lightweight CNN model to preprocess the

images using background elimination. This method optimizes the number of convolutional operations performed by the CNN module to reduce the complexity of the model and maintain accuracy. The YOLO series is the most popular algorithm among CNN-based one-stage detectors in recent years. Zhao et al. [18] proposed a deep learning-based vehicle detection method that improves detection performance by improving YOLOv4, suppressing irrelevant information using an attention mechanism, and modifying the neck network to enhance feature extraction during downsampling to improve the performance of the model for detection and classification. Dong et al. [19] proposed a lightweight YOLOv5 vehicle detection method, which adds C3Ghost and Ghost modules to the neck network to reduce the weight of the model, CBAM modules to the backbone network to improve the detection accuracy, and uses the CIoU loss function to speed up the regression, achieving good results on the PASCAL VOC and MS COCO datasets. Bie et al. [20] improved the YOLOv5n and proposed the YOLOv5n-L model. The model uses depth-separable convolution and C3Ghost module instead of C3 module to reduce parameters, incorporates SE attention mechanism to improve detection accuracy, uses BiFPN for multi-scale feature fusion to enrich feature information, and finally lowers model weights to improve detection.

But these methods mentioned above are either slow detection, poor detection accuracy, or difficult to deploy. In this paper, we propose a lightweight YOLOv7-tiny vehicle detection model called Ghost-YOLOv7. The model in this paper uses an efficient and straightforward structure instead of an inefficient and complex one to improve detection accuracy while lightweight the model structure to achieve accurate real-time detection of objects. The main contributions of this paper are as follows:

- (1) The width factor of the YOLOv7-tiny network is scaled to 0.5, and Ghost convolution is used to replace the standard convolution of the backbone network to achieve a lighter model and improve the detection speed.
- (2) A Ghost-BiFPN neck network is designed to enhance the feature extraction capability of the network and enrich the network information.
- (3) A lightweight Ghost Decoupled Head is proposed to make the classification and localization of detection heads more focused on the information they need and speed up the model's convergence.
- (4) A coordinate attention mechanism is used to improve the focus on the vital information of the vehicle detection task, and a WIoU loss function is introduced to improve the detection accuracy of the algorithm.

The remainder of this paper is organized as follows: Section 2 describes the principle of YOLOv7-tiny and the details of the Ghost-YOLOv7 model. Section 3 describes the ablation experiments and the comparative analysis under different data sets. Section 4 summarizes the work of this paper.

2、Method

2.1. YOLOv7-tiny architecture

YOLOv7 [21] is one of the most popular one-stage object detection networks. YOLOv7-tiny is the most miniature model in the YOLOv7 version, and its backbone network consists of ELAN structures and Downsampling modules. The input image is passed through the backbone network to generate three feature maps of different sizes, passed into the neck network to further enhance the feature fusion capability, and finally passed through the detection head to get the final detection result. Although the YOLOv7-tiny model shows great detection accuracy and speed in lightweight models, these problems still exist as follows:

- (1) YOLOv7-tiny model for traffic detection in autonomous driving, the number of parameters of the model and the amount of computation are too high to be deployed to the on-board edge computing platform.
- (2) The three detection heads of YOLOv7-tiny detect small and large objects. Still, the low resolution of small objects and the insufficient semantic information obtained from the feature maps lead to the poor detection of small objects by YOLOv7-tiny.
- (3) The environment of traffic detection is complex and variable, and the YOLOv7-tiny algorithm is vulnerable to missed and false detections in this environment.

2.2. Ghost-YOLOv7 architecture

In response to the shortcomings of the YOLOv7-tiny algorithm, this paper improves it and names the improved model Ghost-YOLOv7. The structure of Ghost-YOLOv7 is shown in Figure 1 and Figure 2. Firstly, this paper changes the width factor of the original YOLOv7-tiny network from 1.0 to 0.5 and replaces the standard convolution in the backbone network with Ghost convolution to achieve a lightweight network; secondly, this paper designs a Ghost-BiFPN neck network to enhance the feature extraction capability of the network; then, a light decoupling head is used for result prediction to improve the model's small object detection capability; finally, this paper also incorporates an attention mechanism and Wise-IoU loss function to improve the detection accuracy further. A detailed explanation of each module is shown below:

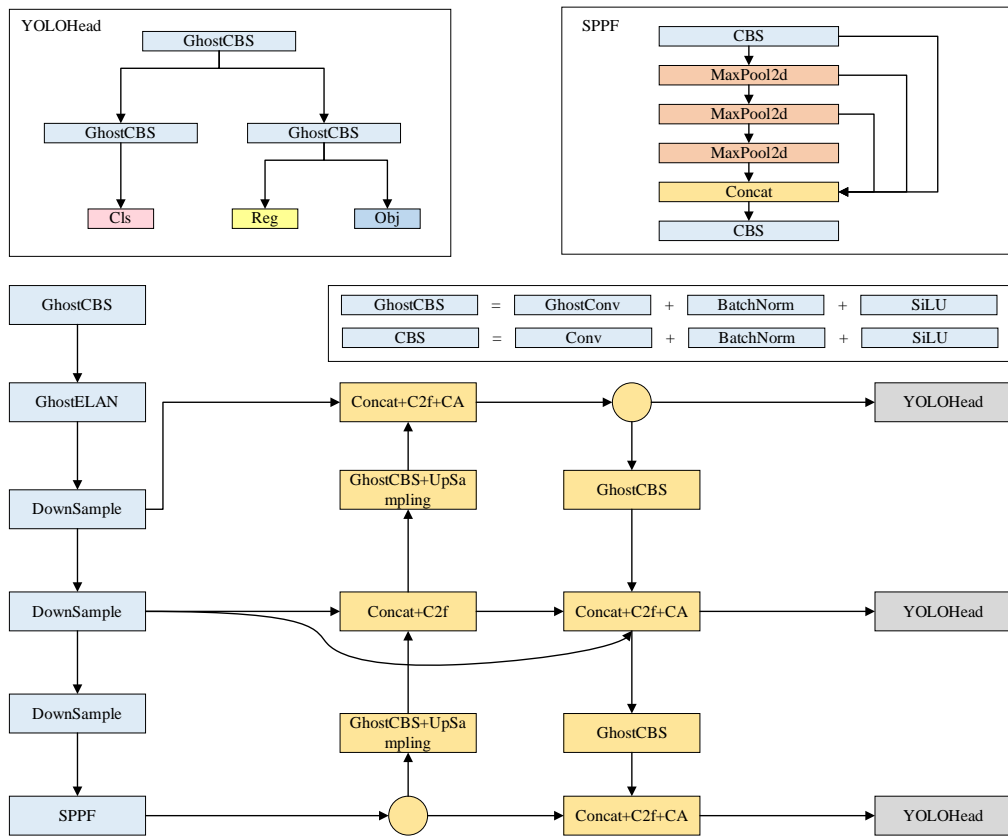


Figure 1 Framework of Ghost-YOLOv7

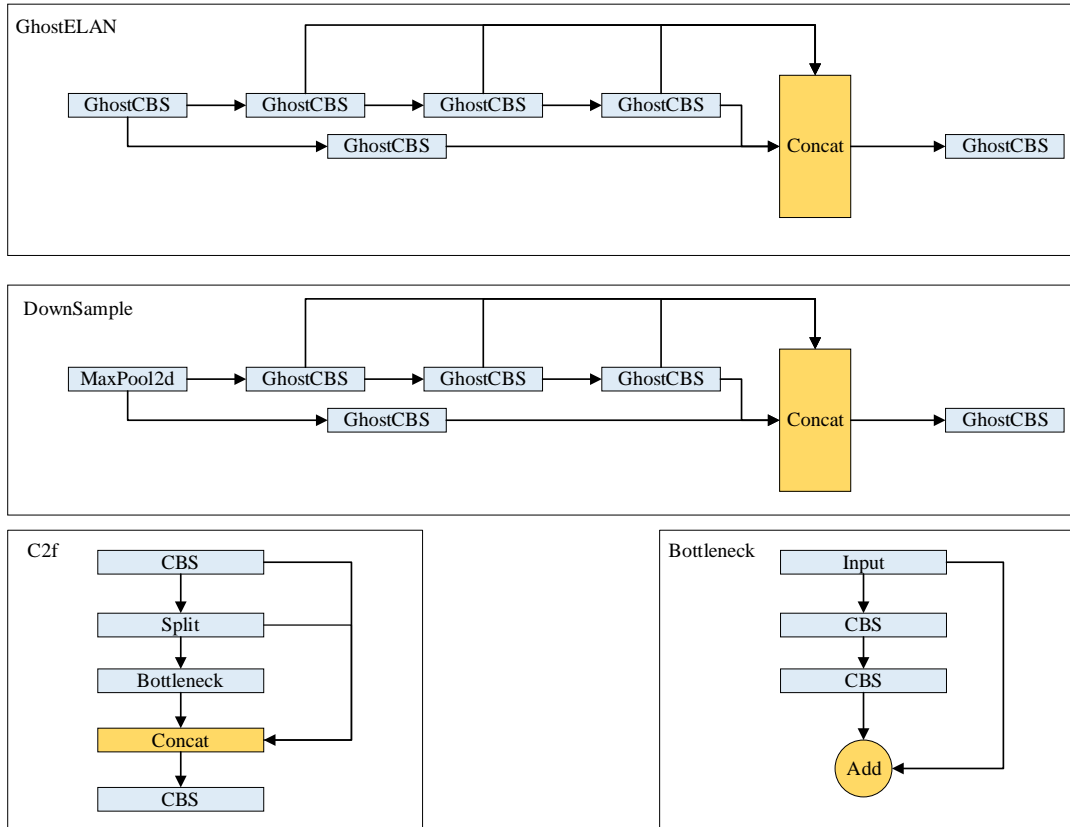


Figure 2 The structure of some modules in Ghost-YOLOv7

2.2.1. GhostConv

Since the calculation power of on-board edge platforms is usually low, we expect the network model to be as small as possible while maintaining accuracy. GhostNet [22] proposes a new Ghost module to generate more feature maps through cheaper operations. In the standard convolution operation, suppose we give input data $X \in R^{h \times w \times c}$, where W and h are the width and height of the input data and c is the number of input channels, respectively. The operation of the convolution layer to generate m feature maps is shown in formula 1:

$$O = X * f + b \quad (1)$$

where b is the bias item, $*$ denotes the convolution operation, $O \in R^{h \times w \times m}$ denotes the output feature map for m channels, and $f \in R^{c \times k \times k \times m}$ is the convolution filter. Furthermore, w' and h' are the width and height of the output data and $k \times k$ denotes the kernel size of convolution filters f . The calculation of the standard convolution can then be formulated as follows:

$$m \cdot w' \cdot h' \cdot c \cdot k \cdot k \quad (2)$$

Since the number of channels and filters in a network is usually large, it can also lead to a massive amount of computation for standard convolution. The Ghost convolution uses inexpensive linear operations to reduce costs compared to standard convolution. Given a linear operator kernel of size $l \times l$, suppose n feature maps are obtained by the original method then $m = n \cdot s$, s represents the corresponding redundant features and $s \ll c$. The operation process of Ghost convolution is shown in Figure 3, there is an identity mapping, and the actual amount of transformation is:

$$n \cdot (s-1) = \frac{m}{s} \cdot (s-1) \quad (3)$$

The computational volume of Ghost convolution can be expressed as:

$$\frac{m}{s} \cdot h' \cdot w' \cdot c \cdot k \cdot k + (s-1) \cdot \frac{m}{s} \cdot h' \cdot w' \cdot l \cdot l \quad (4)$$

The computational saving of using Ghost convolution instead of standard convolution is:

$$\begin{aligned} & \frac{\frac{m}{s} \cdot h' \cdot w' \cdot c \cdot k \cdot k + (s-1) \cdot \frac{m}{s} \cdot h' \cdot w' \cdot l \cdot l}{m \cdot h' \cdot w' \cdot c \cdot k \cdot k} \\ &= \frac{\frac{1}{s} \cdot c \cdot k \cdot k + \frac{s-1}{s} \cdot l \cdot l}{c \cdot k \cdot k} \approx \frac{s+c-1}{s \cdot c} \approx \frac{1}{s} \end{aligned} \quad (5)$$

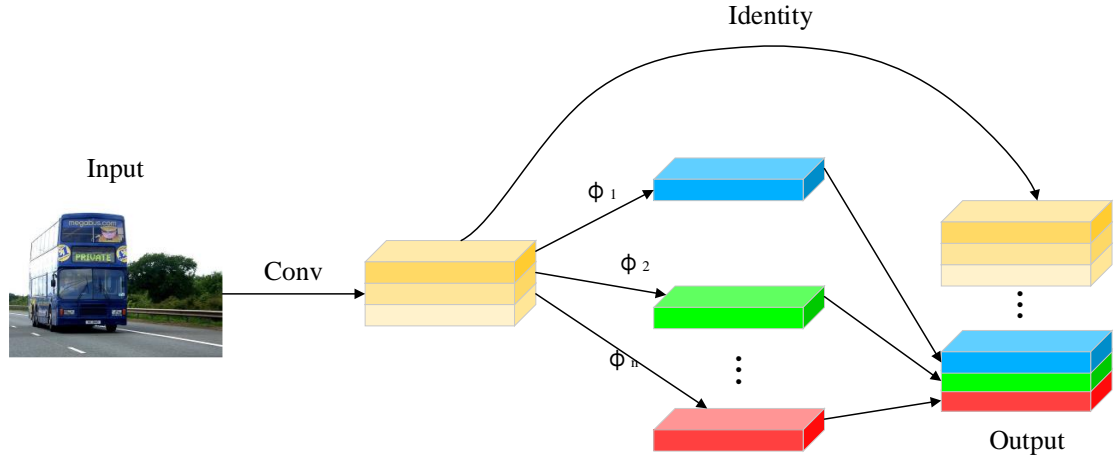


Figure 3 The Ghost convolutional

2.2.2. Ghost-BiFPN

In this section, a lightweight neck network named Ghost-BiFPN is designed in this paper. Ghost-BiFPN combines the neck network of YOLOv5 and YOLOv8, adds BiFPN [23], and uses Ghost convolution instead of standard convolution to reinforce the feature fusion capability of the network and the robustness of the feature map. YOLOv7 combines FPN and PAN [24] for feature fusion, the same as YOLOv5. In vehicle detection, there are different types of vehicles, which all have different shapes and sizes. The combination of FPN and PAN fails to fully utilize the features with different resolutions, so this paper uses BiFPN for the neck network.

The basic idea of bidirectional feature pyramid networks is efficient bidirectional cross-scale connections and weighted feature fusion. As shown in Figure 4, three different sizes of feature maps are input from the backbone network. The features of P3 and P1 are fused directly to the output, which has only one output edge in both stages and has little effect on merging different feature information. Second, an additional edge is added to the output node at this layer of P2, represented by the red line, to fuse more features without increasing the computational cost. Finally, the connection between the input layer of P3 and P2 and the output layer of P1 is added to obtain a higher level of feature fusion.

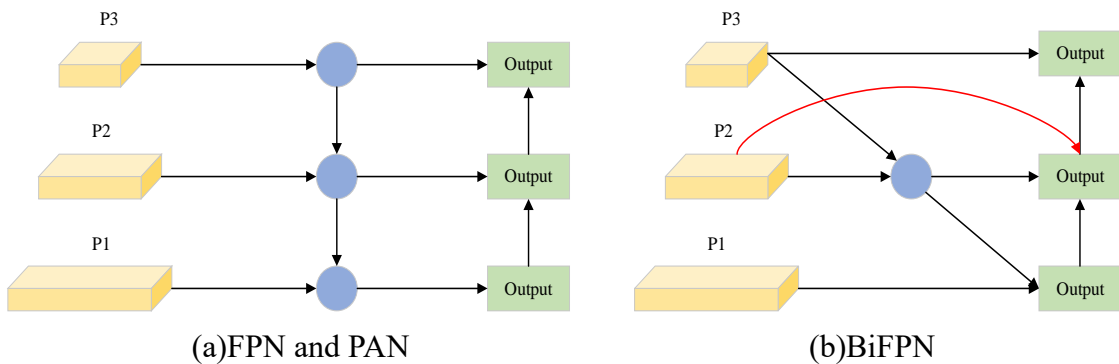


Figure 4 The BiFPN structure

When fusing features of different resolutions, it is common practice to adjust them

to the exact solution and then sum them up. However, since the explanations of varying input features are different, the weights of their output features are different. Therefore, in this paper, an extra weight is added to each input of BiFPN to make the network learn the importance of each input feature. We use fast normalized fusion to adjust the weights in BiFPN, as shown in equation 6:

$$O = \sum_i \frac{w_i}{\varepsilon + \sum_j w_j} \cdot I_i \quad (6)$$

where w_i is a learnable weight and $w_i \geq 0$ is guaranteed by applying a SiLU after each w_i , and $\varepsilon = 0.0001$ is to prevent the value from being instability. Similar to the softmax-based fusion approach, each value of the normalized weights is between 0 and 1. The output feature map of each module of BiFPN can be represented as:

$$P_1^{out} = C\left(\frac{w_1 \cdot P_1^{in} + w_2 \cdot R(P_2^{td})}{w_1 + w_2 + \varepsilon}\right) \quad (7)$$

$$P_2^{out} = C\left(\frac{w_1 \cdot P_2^{in} + w_2 \cdot P_2^{td} + w_3 \cdot R(P_1^{out})}{w_1 + w_2 + w_3 + \varepsilon}\right) \quad (8)$$

$$P_3^{out} = C\left(\frac{w_1 \cdot P_3^{in} + w_2 \cdot R(P_2^{out})}{w_1 + w_2 + \varepsilon}\right) \quad (9)$$

where the output feature map at P1, P2 and P3 are denoted by P_1^{out} , P_2^{out} and P_3^{out} respectively. The P_1^{in} , P_2^{in} and P_3^{in} are denoted the input feature map at P1, P2, and P3 respectively, C is denoted convolution operation, w_1 , w_2 and w_3 represent the weights of each layer and R is resizing operation. The intermediate feature P_2^{td} can be represented as:

$$S_2^{td} = C\left(\frac{w_1 \cdot S_2^{in} + w_2 \cdot R(S_3^{in})}{w_1 + w_2 + \varepsilon}\right) \quad (10)$$

where w_1 and w_2 are the corresponding weights.

2.2.3. Ghost Decoupled Head

The detection head of YOLOv7-tiny uses the same coupled head as YOLOv5. Still, in object detection, the information on classification and localization concerns are different, so the decoupled head performs operations on other branches to improve detection accuracy.

In the model of this paper, combining the decoupled head of YOLOX [25] and the efficient decoupled head of YOLOv6 [26], we propose a lightweight Ghost decoupled head. Specifically, we reduce the number of 3×3 convolutional layers in YOLOX to one and replace the standard 3×3 convolutional layers with Ghost convolution, effectively

reducing the computational cost. The structure of the Ghost decoupled head is shown in Figure 6.

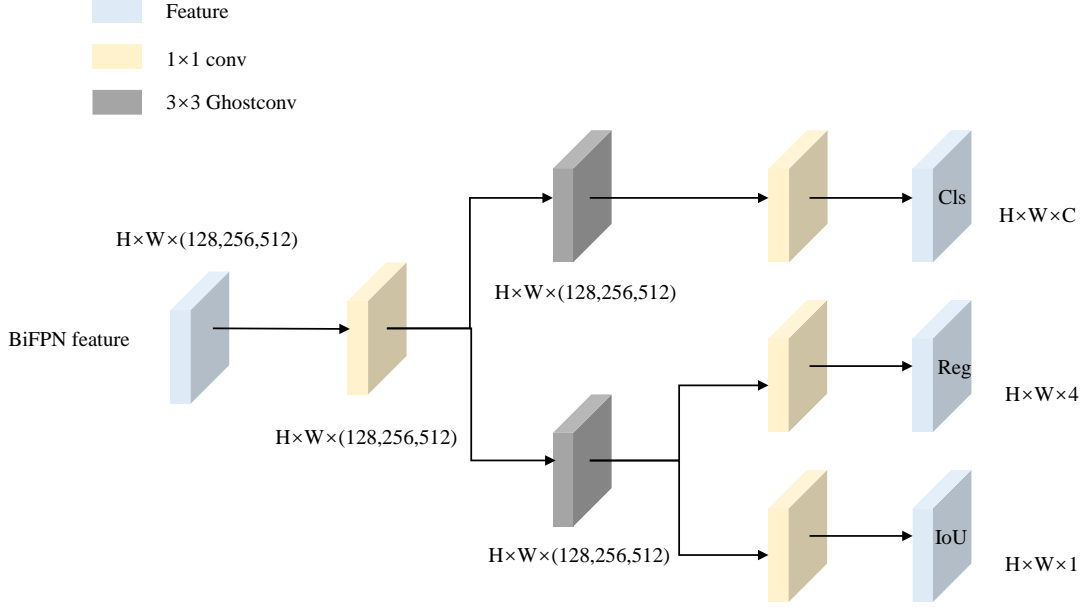


Figure 5 The structure of the Ghost decoupled head

2.2.4. Coordinate attention mechanism

In the vehicle detection of complex scenes, the detection of too many objects and the complexity of the locations will lead to the loss of information in the network. Hence, this paper adds coordinate attention mechanism [27] in the network to make the network pay more attention to the detected target information and suppress some irrelevant information. SE attention mechanisms prove that channel attention has a good effect on improving model performance. Still, they usually ignore location information, which is also considered necessary for spatial feature maps by coordinate attention mechanisms.

The coordinate attention mechanism can be seen as a computational unit that aims to enhance feature representation in the network, which encodes channel relations and long-term dependencies through precise location information. A global average pooling decomposition is first performed, decomposed into two one-dimensional feature encoding operations by two pooling kernels. The first channel is encoded with a pooling kernel of size $(H, 1)$ along the horizontal coordinates for the channel. For a given input X , the

output of the c_{th} channel at height h is shown in Equation 11:

$$z_c^h(h) = \frac{1}{W} \sum_{0 \leq i < W} x_c(h, i) \quad (11)$$

The other channel is encoded with a pooling kernel of size $(1, W)$ along the vertical coordinates of the channel. The output of the c_{th} channel at width w is shown in Equation 12:

$$z_c^w(w) = \frac{1}{H} \sum_{0 \leq j < H} x_c(j, w) \quad (12)$$

The above two transformations aggregate features along two spatial directions to obtain the corresponding direction-aware feature maps. The global perceptual field can be well obtained by these two transformations and encode the precise location information. To utilize the representations generated by the transformations, a second transformation is proposed, where the above transformations are subjected to a stacking operation and then transformed with a 1×1 convolutional transform function F_1 as shown in equation 13:

$$f = \delta(F_1([z^h, z^w])) \quad (13)$$

where $[z^h, z^w]$ denotes the stacking operation along the vertical and horizontal directions, δ is the nonlinear activation function, and f is the intermediate feature map encoded along the horizontal and vertical directions. Then f is decomposed into two independent tensors along the spatial dimension. The number of channels is converted to a size consistent with the number of channels of the input X using two 1×1 convolutions. The conversion process is shown in Equation 14 and Equation 15:

$$g^h = \sigma(F_h(f^h)) \quad (14)$$

$$g^w = \sigma(F_w(f^w)) \quad (15)$$

where F_h and F_w represent the 1×1 convolution, σ is the sigmoid activation function, and the obtained g^h and g^w are used as the attention weights. Finally, the output of the coordinate attention module is shown in Equation 16, and the structure of the coordinate attention module is shown in Figure 5.

$$y_c(i, j) = x_c(i, j) \times g_c^h(i) \times g_c^w(j) \quad (16)$$

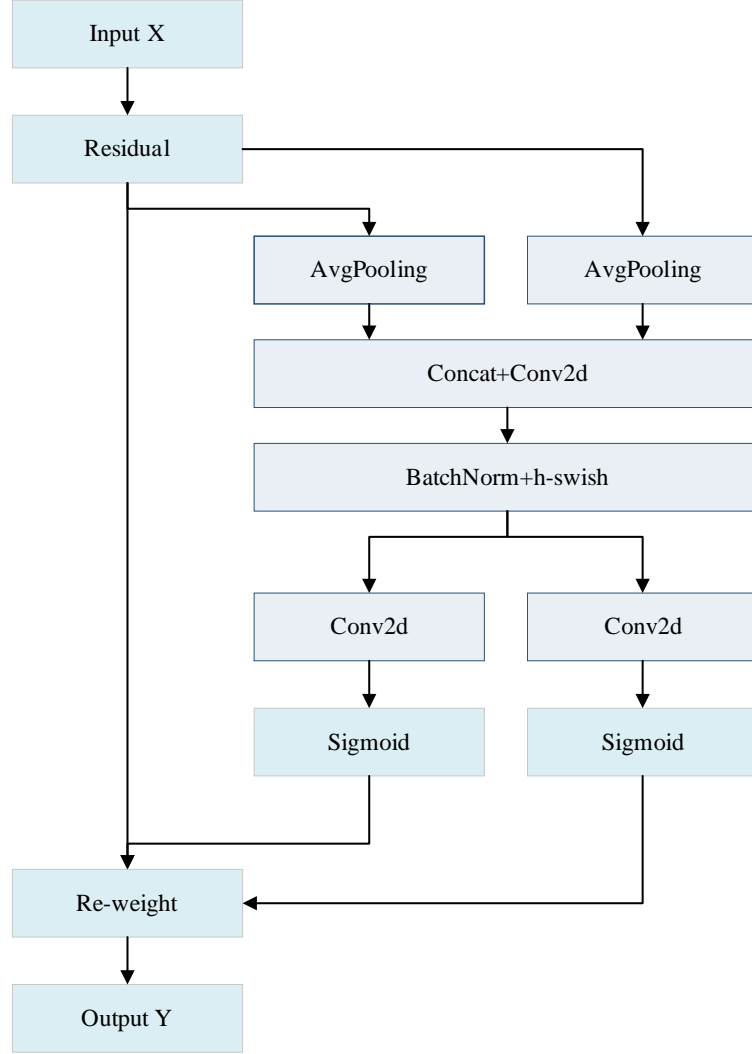


Figure 6 The coordinate attention mechanism structure

2.2.5. Loss function improvement

The loss function of YOLOv7-tiny consists of three components: the confidence loss l_{obj} , the classification loss l_{cls} , and the bounding box loss l_{box} , where the bounding box loss consists of bounding box position loss and bounding box prediction loss. The calculation formula of the loss function can be expressed as:

$$\text{Loss} = l_{obj} + l_{cls} + l_{box} \quad (17)$$

The confidence loss can be denoted as:

$$\begin{aligned}
 l_{obj} &= \sum_{i=0}^{s^2} \sum_{j=0}^B I_{ij}^{obj} (\hat{C}_i \log(C_i) + (1 - \hat{C}_i) \log(1 - \hat{C}_i)) - \\
 &\quad \lambda_{noobj} \sum_{i=0}^{s^2} \sum_{j=0}^B I_{ij}^{noobj} (\hat{C}_i \log(C_i) + (1 - \hat{C}_i) \log(1 - \hat{C}_i))
 \end{aligned} \quad (18)$$

The classification loss can be shown by equation 19:

$$l_{cls} = \sum_{i=0}^{s^2} l_{ij}^{obj} \sum_{c \in classes} (\hat{P}_i(c) \log(P_i(c)) + (1 - \hat{P}_i(c)) \log(1 - P_i(c))) \quad (19)$$

The CIoU [28] loss function is used for regression prediction of the bounding box:

$$Loss_{IoU} = 1 - IoU, IoU = \frac{|A \cap B|}{|A \cup B|} \quad (20)$$

$$Loss_{CIoU} = 1 - IoU + \frac{\rho_{(b, b^{gt})}^2}{d^2} + \alpha v \quad (21)$$

where the parameters A and B represent the areas of the ground-truth and prediction bounding boxes; b, b^{gt} represent the centroids of the prediction and ground-truth bounding boxes, respectively; ρ represents the Euclidean distance between the two centroids; d is the diagonal distance of the smallest enclosing region that can contain both the prediction and ground-truth bounding boxes; α is the weight function; v is used to measure the similarity of the aspect ratios. The expression of α and v is as follows:

$$\alpha = \frac{v}{(1 - IoU) + v} \quad (22)$$

$$v = \frac{4}{\pi^2} \left(\arctan \frac{w^{gt}}{h^{gt}} - \arctan \frac{w}{h} \right)^2 \quad (23)$$

Although the CIoU loss function solves the problem of gradient disappearance that may be caused by the IoU loss function during training by considering factors such as aspect ratio, there is still room for optimization. The WIoU [29] loss function evaluates the quality of the anchor box by replacing IoU with an outlier degree through a dynamic non-monotonic focusing mechanism and proposes a wise gradient gain allocation strategy that significantly improves the performance. The equation for the WIoU loss function is shown below:

$$Loss_{WIoU} = r \cdot \exp \left(\frac{\rho_{(b, b^{gt})}^2}{(d^2)^*} \right) \cdot (1 - IoU) \quad (24)$$

$$r = \frac{\beta}{\delta \alpha^{\beta - \delta}}, \beta = \frac{(1 - IoU)^*}{1 - IoU} \in [0, +\infty) \quad (25)$$

where $*$ indicates that the dimensions of the smallest bounding box are detached from the computational graph; β is the outlier degree; α and δ are the hyperparameters, where we take $\alpha = 1.9$ and $\delta = 3$.

In contrast to the CIoU loss function, the WIoU loss function uses an outlier degree to dynamically adjust the anchor box's gradient gain to improve the anchor box's gradient gain as much as possible during the training to achieve the improvement of detection accuracy.

3、Experiment

3.1. Dataset

For the complex environment in traffic scenarios, the diversity of vehicles as well as weather, the work in this paper is studied on three datasets, which are Pascal VOC2007+2012 [30], KITTI [31], and BIT-Vehicle [32]. Each dataset will be described in detail in subsequent sections of this paper.

3.2. Experimental environment and evaluation indicators

The hardware environment for the experiments in this paper is as follows: CPU is Intel Core i5-11400; GPU is Nvidia GeForce RTX 3060Ti, 8G display memories. The software environment for the experiments in this paper is as follows: The operating system is Ubuntu 18.04, the CUDA version is 11.3, the programming language is Python 3.8, and the deep learning framework is Pytorch 1.12.1. For the training details, the optimizer is used with Adam; the initial learning rate is 0.001; the number of training epochs is set to 100; the batch size is set to 16; the input size of the image is set to 640×640 , and the IoU threshold is set to 0.5. To speed up the convergence of the models, each model uses weights pre-trained on ImageNet.

The model validation in this paper uses mean average precision(mAP), frames per second(FPS), number of parameters, and the floating point operations (FLOPs). The mAP is frequently used to evaluate the model's accuracy in object detection. It depends on the average precision(AP) and IoU. While AP depends on precision and recall, they can be expressed as:

$$P(\text{precision}) = \frac{TP}{TP + FP} \quad (26)$$

$$R(\text{recall}) = \frac{TP}{TP + FN} \quad (27)$$

$$AP = \int_0^1 P(R) dR \quad (28)$$

$$mAP = \frac{1}{n} \sum_{i=1}^n \int_0^1 P(R) dR \quad (29)$$

where TP denotes true positive, FP denotes false positive, FN denotes false negatives, and n is the number of categories. FPS represents the model's speed on the platform, while the number of parameters and the FLOPs measure the computational cost.

3.3. Results of ablation experiments

In this section, ablation experiments will be performed to verify the model's validity in this paper. The ablation experiments in this paper are conducted on Pascal

VOC2007+2012. Since 20 categories exist in the dataset of the Pascal VOC series itself, only five categories commonly found in traffic scenes are extracted in this paper: bicycle, motorbike, bus, car, and person. Since the number of extracted datasets is not large enough, this paper combines VOC2007 and VOC2012 to obtain a total of 16,441 images, which are divided into the training set, validation set, and test set according to 8:1:1.

As shown in the table below, Table 1 shows the models generated by different improvement methods, and Table 2 shows the results of the ablation experiments. In this paper, we first adjust the width multiple of the network to 0.5. Table 2 shows that the number of parameters and computation of the model and the model size is reduced by nearly four times compared with the original model. Then the standard convolution of the backbone network is replaced by Ghost convolution to lighten the network further. To enhance the detection accuracy of the model, Ghost-BiFPN is used to improve the feature fusion capability of the network, and it can be seen that Ghost-BiFPN increases the number of parameters and computation of the model by a small amount, which significantly improves the detection accuracy. Finally, WIoU loss function, coordinate attention mechanism, and GDH is added to improve detection accuracy. Compared with the original model, Ghost-YOLOv7 has 37.3% fewer parameters, 29.8% less computation, 35.1% less model size, and 1.1% more mAP, and the improved model has a detection speed of 428 FPS on the test dataset when the batch size(bs) is set to 16.

Table 1 The combination of different improvement methods results.

Improvement methods	Model1	Model2	Model3	Model4	Model5	Model6
YOLOv7t-0.5width	✓	✓	✓	✓	✓	✓
YOLOv7t-Ghost-Backbone		✓	✓	✓	✓	✓
YOLOv7t-Ghost-BiFPN			✓	✓	✓	✓
YOLOv7t-CA				✓	✓	✓
YOLOv7t-WIoU					✓	✓
YOLOv7t-GDH						✓

Table 2 Comparison of ablation experiments of the overall model.

Model	Params(M)	FLOPs(B)	mAP@0.5(%)	Weight(MB)	FPS(bs=16)
YOLOv7-tiny	6.01	13.1	80.5	11.7	401
model1	1.51	3.4	74.6	3.1	500
model2	1.33	3.0	74.2	2.8	525
model3	2.00	4.4	78.1	4.0	481
model4	2.01	4.4	79.3	4.0	461
model5	2.00	4.4	80.1	4.0	461
model6	3.77	9.2	81.6	7.6	428

3.4. Comparison analysis of algorithms

3.4.1. performance on the Pascal VOC2007+2012 dataset

The VOC 2007 and 2012 datasets are recognized as challenging object detection datasets. There are 9963 images in the VOC2007 dataset, containing 20 categories, and 11530 images in the VOC2012 dataset, also containing 20 categories. The proposed algorithm in this paper is mainly used for vehicle detection in complex environments, so only five categories in the traffic scenes are extracted. This section compares the different algorithms on this dataset. As shown in Table 3, Ghost-YOLOv7 achieves the highest detection speed of 428 FPS. Although the number of parameters and computation of the model is more prominent than YOLOv5n, Ghost-YOLOv7 also has the highest detection accuracy among the lightweight models. The detection results are shown in Figure 7. Comparing the original algorithm YOLOv7-tiny, it can be seen that Ghost-YOLOv7 is better for small targets and more robust at multiple objects.

Table 3 Comparison results of different algorithms on the VOC2007+2012 dataset.

Model	Params(M)	FLOPs(B)	mAP@0.5(%)	Weight(MB)	FPS(bs=16)
YOLOv7-tiny	6.01	13.1	80.5	11.7	401
YOLOv5n	1.76	4.1	77.3	3.8	385
YOLOv3-tiny	8.67	12.9	63.1	16.6	345
Faster R-CNN	137.07	626.2	78.2	521.0	14
Ghost-YOLOv7	3.77	9.2	81.6	7.6	428



Figure 7 Comparison of the detection results of Ghost-YOLOv7 and YOLOv7-tiny on the VOC2007+2012 dataset. The top is the Ghost-YOLOv7 model, and the bottom is the YOLOv7-tiny model.

3.4.2. performance on the KITTI dataset

The KITTI dataset installs vehicle cameras to capture image data from urban, rural, and highway scenarios. The dataset consists of 7481 images and contains five categories: car, people, cyclist, van, and truck, but in the evaluation phase, it officially only considers three categories of car, people, and cyclist. Since the ground truth of the test set is not officially provided, this paper divides the training and test sets into 3712 and 3769 images. The evaluation of the KITTI dataset is classified as easy, moderate, and complicated according to the bounding box's height and the occlusion level. As shown in Table 4, Ghost-YOLOv7 achieved 88.4% mAP on the KITTI dataset, which is a 1% improvement in mAP compared to YOLOv7-tiny, and also performed better at all three different difficulty levels. Overall, Ghost-YOLOv7 detects better on targets of various sizes, and Figure 8 shows the detection effect images.

Table 4 Comparative analysis of different algorithms on the KITTI dataset. E stands for Easy, M stands for Moderate, and H stands for Hard.

Model	AP(%)									mAP(%)	FPS(bs=16)		
	Car			Person			Cyclist						
	E	M	H	E	M	H	E	M	H				
YOLOv7-tiny	97.6	90.0	88.5	87.3	78.5	77.1	89.5	87.5	80.1	87.4	401		
YOLOv5n	97.1	89.6	80.5	84.3	76.2	74.6	87.9	79.5	78.8	85.7	385		
YOLOv3-tiny	90.1	85.4	76.4	81.5	73.3	66.4	83.1	75.2	74.4	79.6	345		
Faster R-CNN	97.1	89.8	79.6	85.1	76.7	75.2	88.2	79.6	78.7	86.1	14		
Ghost-YOLOv7	97.4	90.1	88.7	87.3	78.7	77.4	89.7	87.7	80.2	88.4	428		



Figure 8 Comparison of detection results of Ghost-YOLOv7 and YOLOv7-tiny on the KITTI dataset. The top is the Ghost-YOLOv7 model, and the bottom is the YOLOv7-tiny model.

3.4.3. performance on the BIT-Vehicle dataset

The BIT-Vehicle dataset is a dataset produced by the Beijing Institute of Technology. The dataset contains a total of 9850 images, most of which have only one to two vehicles, and the dataset as a whole is relatively simple. The dataset is divided into six categories:

bus, microbus, minivan, sedan, SUV, and truck. In this paper, the dataset is divided into the training set, validation set, and test set according to 8:1:1, and the experimental results are shown in Table 5. The proposed model in this paper achieves 99.1% mAP, which is a good improvement in all aspects compared to the original model. As shown in Figure 9, Ghost-YOLOv7 has a higher detection effect and better detection in the face of obscured targets.

Table 5 Experimental results of different algorithms on the BIT-Vehicle dataset.

Model	Params(M)	FLOPs(B)	mAP@0.5(%)	Weight(MB)	FPS(bs=16)
YOLOv7-tiny	6.01	13.1	98.5	11.7	401
YOLOv5n	1.76	4.1	98.0	3.8	385
YOLOv3-tiny	8.67	12.9	97.8	16.6	345
Faster R-CNN	137.07	626.2	98.1	521.0	14
Ghost-YOLOv7	3.77	9.2	99.1	7.6	428

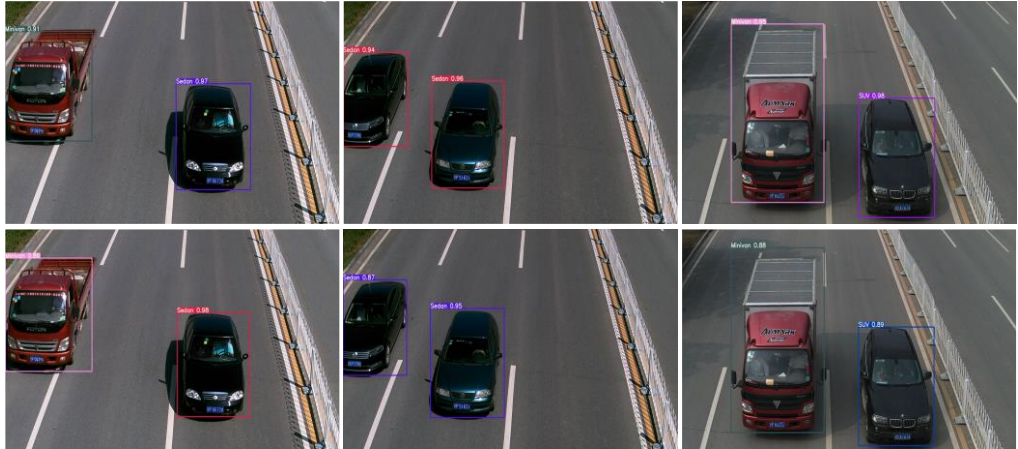


Figure 9 Comparison of the detection results of Ghost-YOLOv7 and YOLOv7-tiny on the BIT-Vehicle dataset. The top is the Ghost-YOLOv7 model, and the bottom is the YOLOv7-tiny model.

4、Conclusion

This paper proposes a lightweight vehicle detection model based on the YOLOv7-tiny model named Ghost-YOLOv7. The model firstly scales the width multiple to 0.5 and uses Ghost convolution to replace the standard convolution of the backbone network, which dramatically reduces the number of parameters and computation of the model and improves the detection speed; secondly, this paper designs a Ghost-BiFPN neck network to enhance the feature fusion capability of the network; then a lightweight Ghost decoupling head is added to improve the convergence speed and detection effect; finally, a coordinate attention mechanism and WIoU loss function are introduced to enhance the detection accuracy further. The model has some application value in a complex traffic environment. The experimental results in this paper on VOC2007+2012, KITTI, and BIT-Vehicle datasets show that Ghost-YOLOv7 has higher detection accuracy and lower computational cost than other detection algorithms in most cases. Follow-up work can be

considered to enhance the model's detection accuracy and deploy the improved model to resource-constrained on-board edge platforms.

CRediT authorship contribution statement

Bo Li: Resources, Writing – review & editing, Supervision. **YiHua Chen:** Investigation, Validation. **Hao Xu:** Conceptualization, Writing – original draft, Software.

Declaration of competing interest

The authors declare that they have no known competing financial interests or personal relationships that could have appeared to influence the work reported in this paper.

Acknowledgments

This research was sponsored by the National Natural Science Foundation of China (Grant No.: 52005168), the Initial Scientific Research Foundation of Hubei University of Technology (BSQD2020005), and the Open Foundation of Hubei Key Lab of Modern Manufacture Quality Engineering (KFJJ-2020009).

References

- [1] Sonata, I., et al. "Autonomous car using CNN deep learning algorithm." *Journal of Physics: Conference Series*. Vol. 1869. No. 1. IOP Publishing, 2021.
- [2] Tsai L W , Hsieh J W , Fan K C . Vehicle Detection Using Normalized Color and Edge Map[J]. *IEEE Transactions on Image Processing*, 2007, 16(3):850-864.
- [3] Chen H T , Wu Y C , Hsu C C . Daytime Preceding Vehicle Brake Light Detection Using Monocular Vision[J]. *IEEE Sensors Journal*, 2015, 16(1):1-1.
- [4] Bai H , Wu J , Liu C . Motion and haar-like features based vehicle detection[C]// *International Multi-media Modelling Conference*. IEEE, 2006.
- [5] Mo G , Yan Z , Zhang S , et al. A Method of Vehicle Detection Based on SIFT Features and Boosting Classifier[J]. *Journal of Convergence Information Technology*, 2012, 7(12):328-334.
- [6] Tian, S. , et al. "Multilingual scene character recognition with co-occurrence of histogram of oriented gradients." *Pattern Recognition* 51.C(2016):125-134.
- [7] Cheng W C , Jhan D M . A self-constructing cascade classifier with AdaBoost and SVM for pedestrian detection[J]. *Engineering Applications of Artificial Intelligence*, 2013, 26(3):1016-1028.
- [8] Satzoda R K , Trivedi M M . Multipart Vehicle Detection Using Symmetry-

Derived Analysis and Active Learning[J]. IEEE Transactions on Intelligent Transportation Systems, 2016, 17(4):926-937.

[9] Razalli H , Ramli R , Alkawaz M H . Emergency Vehicle Recognition and Classification Method Using HSV Color Segmentation[C]// 2020 16th IEEE International Colloquium on Signal Processing & Its Applications (CSPA). IEEE, 2020.

[10] LeCun Y, Bottou L, Bengio Y, et al. Gradient-based learning applied to document recognition[J]. Proceedings of the IEEE, 1998, 86(11): 2278-2324.

[11] Vaswani A, Shazeer N, Parmar N, et al. Attention is all you need[J]. Advances in neural information processing systems, 2017, 30.

[12] Dosovitskiy A, Beyer L, Kolesnikov A, et al. An image is worth 16x16 words: Transformers for image recognition at scale[J]. arXiv preprint arXiv:2010.11929, 2020.

[13] Sun Z, Liu C, Qu H, et al. A novel effective vehicle detection method based on Swin Transformer in hazy scenes[J]. Mathematics, 2022, 10(13): 2199.

[14] Deshmukh P, Satyanarayana G S R, Majhi S, et al. Swin transformer based vehicle detection in undisciplined traffic environment[J]. Expert Systems with Applications, 2023, 213: 118992.

[15] Arora N, Kumar Y, Karkra R, et al. Automatic vehicle detection system in different environment conditions using fast R-CNN[J]. Multimedia Tools and Applications, 2022, 81(13): 18715-18735.

[16] Satyanarayana G S R, Deshmukh P, Das S K. Vehicle detection and classification with spatio-temporal information obtained from CNN[J]. Displays, 2022, 75: 102294.

[17] Zakaria C ,Amal E ,Mounir G , et al. A Resource-Efficient CNN-Based Method for Moving Vehicle Detection[J]. Sensors,2022,22(3).

[18] Zhao J, Hao S, Dai C, et al. Improved vision-based vehicle detection and classification by optimized YOLOv4[J]. IEEE Access, 2022, 10: 8590-8603.

[19] Dong X, Yan S, Duan C. A lightweight vehicles detection network model based on YOLOv5[J]. Engineering Applications of Artificial Intelligence, 2022, 113: 104914.

[20] Bie M, Liu Y, Li G, et al. Real-time vehicle detection algorithm based on a lightweight You-Only-Look-Once (YOLOv5n-L) approach[J]. Expert Systems with Applications, 2023, 213: 119108.

[21] Wang C Y, Bochkovskiy A, Liao H Y M. YOLOv7: Trainable bag-of-freebies sets new state-of-the-art for real-time object detectors[J]. arXiv preprint arXiv:2207.02696, 2022.

[22] Han K, Wang Y, Tian Q, et al. Ghostnet: More features from cheap operations[C]//Proceedings of the IEEE/CVF conference on computer vision and pattern recognition. 2020: 1580-1589.

[23] Tan M, Pang R, Le Q V. Efficientdet: Scalable and efficient object detection[C]//Proceedings of the IEEE/CVF conference on computer vision and pattern recognition. 2020: 10781-10790.

[24] Liu S, Qi L, Qin H, et al. Path aggregation network for instance

segmentation[C]//Proceedings of the IEEE conference on computer vision and pattern recognition. 2018: 8759-8768.

[25] Ge Z, Liu S, Wang F, et al. Yolox: Exceeding yolo series in 2021[J]. arXiv preprint arXiv:2107.08430, 2021.

[26] Li C, Li L, Jiang H, et al. YOLOv6: A single-stage object detection framework for industrial applications[J]. arXiv preprint arXiv:2209.02976, 2022.

[27] Hou Q, Zhou D, Feng J. Coordinate attention for efficient mobile network design[C]//Proceedings of the IEEE/CVF conference on computer vision and pattern recognition. 2021: 13713-13722.

[28] Zheng Z, Wang P, Ren D, et al. Enhancing geometric factors in model learning and inference for object detection and instance segmentation[J]. IEEE Transactions on Cybernetics, 2021, 52(8): 8574-8586.

[29] Tong Z, Chen Y, Xu Z, et al. Wise-IoU: Bounding Box Regression Loss with Dynamic Focusing Mechanism[J]. arXiv preprint arXiv:2301.10051, 2023.

[30] Everingham M, Van Gool L, Williams C K I, et al. The pascal visual object classes (voc) challenge[J]. International journal of computer vision, 2010, 88: 303-338.

[31] Geiger A, Lenz P, Urtasun R. Are we ready for autonomous driving? the kitti vision benchmark suite[C]//2012 IEEE conference on computer vision and pattern recognition. IEEE, 2012: 3354-3361.

[32] Dong Z, Wu Y, Pei M, et al. Vehicle type classification using a semisupervised convolutional neural network[J]. IEEE transactions on intelligent transportation systems, 2015, 16(4): 2247-2256.